Postprint of: Bochentyn B., Chlipała M., Gazda M., Wang S.-F., Jasiński P., Copper and cobalt co-doped ceria as an anode catalyst for DIR-SOFCs fueled by biogas, Solid State Ionics, Vol. 330 (2019), pp. 47-53, DOI: 10.1016/j.ssi.2018.12.007

Copper and cobalt co-doped ceria as an anode catalyst for DIR-SOFCs fueled by biogas

B.Bochentyn[1*], M.Chlipała[1], M.Gazda[1], S.-F.Wang[2], P.Jasiński[3]

1. Faculty of Applied Physics and Mathematics, Gdansk University of Technology, 80-233 Gdańsk, ul. Narutowicza 11/12 Poland
2. Department of Material and Mineral Resources Engineering, National Taipei University of Technology, 1, Sec. 3, Zhongxiao E. Rd., Taipei, 106 Taiwan
3. Faculty of Electronics, Telecommunications and Informatics, Gdansk University of Technology, 80-233 Gdańsk, ul. Narutowicza 11/12 Poland

Corresponding author: beata.bochentyn@pg.edu.pl

Abstract

The nanocrystalline compounds of Co and Cu co-doped ceria (with up to 20 mol.% of dopants) were fabricated by the reverse microemulsion synthesis method. They were deposited in a form of layers on the surface of SOFC anode in an aim to act as electrochemically active materials for biogas reforming process. Fourier Transformed Infrared Spectroscopy was used to analyze a composition of outlet gases simultaneously with the tests of electrical parameters of a fuel cell. It allowed comparing a catalytic activity of fabricated materials towards internal biogas reforming. It was found that Cu and Co ceria co-doping improves electrical parameters of a fuel cell and enhances its long-term stability when compared with mono-doped ceria. This type of a material gives also the highest conversion rate of methane and the highest yield of carbon monoxide.

Keywords: biogas reforming, direct internal reforming, carbon deposition, SOFC, FTIR.

1. Introduction

Biogas usually consists of methane (40–65%), carbon dioxide (30–40%) and a trace amount of nitrogen, hydrogen, hydrogen sulfide and oxygen. It can act as a fuel for Solid Oxide Fuel Cells where a direct internal reforming of hydrocarbons (DIR-SOFC) and an activation of electrochemical reactions occurs on the anode. Possible reactions of this process are presented in Table 1:

Table 1: Possible reactions in porous anode material of SOFC within the direct internal reforming of biogas [1-3].

(1)	Dry reforming of CH_4	$CH_4+CO_2 \leftrightarrow 2CO+2H_2$
(2)	Reverse water-gas shift	$CO_2+H_2 \leftrightarrow CO+H_2O$
(3)	Methanation	$CO_2+4H_2 \leftrightarrow CH_4+2H_2O$
(4)	Steam reforming of CH_4	$CH_4+H_2O \leftrightarrow CO+3H_2$
(5)	CH_4 pyrolysis	$CH_4 \leftrightarrow C_{solid}+2H_2$
(6)	CO dysproportionation (Boudouard reaction)	$2CO \leftrightarrow C_{solid}+CO_2$
(7)	CO reduction	$CO+H_2 \leftrightarrow C_{solid}+H_2O$
(8)	Electrochemical oxidation of H_2	$H_2+O^{2-} \leftrightarrow H_2O+2e^-$
(9)	Electrochemical oxidation of CO	$CO+O^{2-} \leftrightarrow CO_2+2e^-$
(10)	Electrochemical oxidation of CH_4	$CH_4+O^{2-} \leftrightarrow 2H_2+CO+2e^-$
(11)	Electrochemical oxidation of solid carbon	$C_{solid}+O^{2-} \leftrightarrow CO+2e^-$

The traditional SOFC Ni-YSZ anode contains a high Ni content (at least 30 vol.%) in order to obtain high electronic conductivity. However, it faces a severe problem of carbon deposition when fuelled with hydrocarbons. Since Ni is a good catalyst for both C-H bond dissociation and C-C bond formation, carbon from methan pyrolysis and CO disproportionation can nucleate and accumulate on highly active sites of Ni catalyst [4]. The performance of the cell would degrade quickly when carbon covers the active sites and blocks the pore channels inside the anode layer. To suppress a carbon formation, the CeO_2-based catalytic materials may be applied to modify commercial SOFC anodes. The high oxygen mobility of ceria promotes the mechanism of carbon removal, which in turn should contribute to the stability of the catalysts on hydrocarbon conversion reactions. Furthermore, doping with cations such as Gd^{3+}, Y^{3+}, Pr^{3+} and Zr^{4+} enhances the mobility of oxygen in

This work was presented during the 13th International Symposium on Systems with Fast Ionic Transport, Minsk, Belarus 03–07.07.2018

ceria and then, increases its oxygen storage capacity (OSC) [5]. These dopants also increase the ionic and electronic conductivity of ceria [5].

Another approach that reduces coking to a high extent is changing the chemical composition of anode itself, which may be obtained by replacing nickel with less reactive elements, such as iron, copper or gold [6-7]. Cobalt is the active component frequently encountered in Fischer-Tropsch synthesis, enabling the dissociative CO adsorption and C-C chain growth and hydrogenation [8]. The main function of copper is enabling the dissociative chemisorption of hydrogen and the un-dissociative adsorption of CO [8]. However, when copper is used to replace nickel in the anode (Cu-YSZ) operating in dry CH_4 fuel, it presents very low activity toward methane oxidation [9-10]. Only when both of these elements are added to ceria, the usage of copper compounds improves the properties of the fuel cells, mainly due to the reduction of carbon deposition while feeding hydrocarbon fuels [9,11]. When CuO-CeO_2 oxide compound is used as an additional layer deposited on the surface of Ni-YSZ anode operating in biogas, it clearly enhances the long-term stability of the fuel cell [12].
In turn, cobalt is expected to present similar to nickel catalytic activity towards oxidation of hydrocarbons but the lower tendency to carbon deposition. Although no performance loss is observed in Co-YSZ anode operating in methane [13], there is a complete delamination of Ni-Co alloy in syngas atmosphere, possibly due to its vulnerability to carbon deposition [14]. In another paper, the Co-Cu/YSZ+CeO_2 system shows a very little carbon deposition in methane containing atmosphere [15] and a controlled deposition of amorphous carbon increasing with increasing metal loading in dry butane [16]. The Co_3O_4/CeO_2 composites are also reported as presenting high catalytic activity towards H_2S decomposition to H_2 [17].

In this work, various nanocrystalline compounds of Co and Cu co-doped ceria (with up to 20 mol.% of dopants) are fabricated by the reverse microemulsion synthesis method. They are deposited in a form of layers on the surface of SOFC anode in aim to act as electrochemically active materials for biogas reforming process. The aim of modification is to investigate an influence of these layers on a lifetime and efficiency of commercially available solid oxide fuel cell operating with biogas without the need of an external reformer.

2. Experimental

Various copper and cobalt doped ceria compounds were synthesized via a reverse microemulsion method. The microemulsion is a thermodynamically stable system of two immiscible liquids, in which one is dispersed in the other. At the interface between these liquids, a thin film formed by surfactant molecules reduces the surface tension between them. A microemulsion in which water is dispersed in the organic phase is called a reverse microemulsion. Water nanoclusters act as nanoreactors in which a synthesis of nanosize materials can be performed.

The following compositions have been fabricated: $Ce_{0.9}Cu_{0.1}O_{2-\delta}$, $Ce_{0.8}Cu_{0.2}O_{2-\delta}$, $Ce_{0.8}Co_{0.1}Cu_{0.1}O_{2-\delta}$, $Ce_{0.8}Co_{0.15}Cu_{0.05}O_{2-\delta}$, $Ce_{0.8}Co_{0.2}O_{2-\delta}$ and $Ce_{0.9}Co_{0.1}O_{2-\delta}$. For this purpose, both cyclohexane (325ml) and pentane-1-ol (52ml) acting as an organic phase and Triton x-100 (58 ml) acting as a non-ionic surfactant were mixed by a magnetic stirrer. In a separate vessel a stoichiometric amount of respective nitrates: $Ce(NO_3)_3 \cdot 6H_2O$, $Co(NO_3)_2 \cdot 6H_2O$ and $Cu(NO_3)_2 \cdot 3H_2O$ was dissolved in water. Then a water phase was mixed with an organic phase and a precipitating agent in a form of tetramethylammonium hydroxide (28 ml) was added. After stirring for 30 minutes a water phase was decanted. The obtained product was centrifuged (4500 rpm for 15 minutes) and rinsed twice with acetone (4500 rpm for 5 minutes) and twice with methanol (4500 rpm for 15 minutes). The dried precipitate was calcined at 500 °C for 2 hours in the air in order to fully crystallize and remove residual nitrates and organic compounds remaining after a synthesis. The phase composition of the investigated materials was analyzed using the X-ray diffraction method (XRD) by an X'Pert Pro MPD Philips diffractometer with Cu Kα (1.542 Å) radiation at room temperature. The size of crystallites was estimated on the basis of the Scherrer formula: $C = k\lambda/[(B_e - B_t)\cos\theta]$, where C is an average diameter of the crystalline grain, k is a constant (assumed to be 0.9), λ is the X-ray wavelength, θ is the diffraction angle, B_e is the measured width of a peak profile and B_t is the instrumental width of a peak. The morphology of fabricated materials was observed using the FEI Quanta FEG 250 Scanning Electron Microscope (SEM).

To form pastes, the obtained powders were ground in a mortar for about 1 hour with ESL 403 organic binder (ElectroScience Laboratory, USA). The prepared pastes were deposited on the anode surface of a traditional 1-inch Solid Oxide Fuel Cell (Ni-YSZ anode, YSZ electrolyte and LSM-YSZ cathode). The scheme of this fuel cell is presented in Fig.1. The catalytic layer was 16 mm in diameter and 30 μm in thickness. Finally, the modified fuel cells with deposited catalytic layers were fired at 1000 °C for 2 h.

This work was presented during the 13th International Symposium on Systems with Fast Ionic Transport, Minsk, Belarus 03–07.07.2018

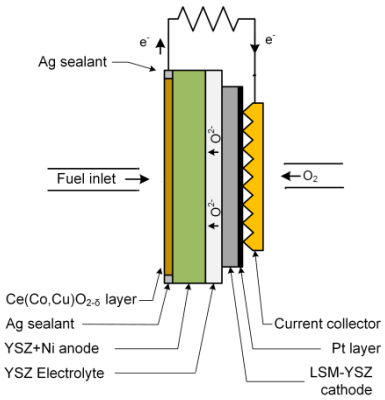

Fig.1: Scheme of the Solid Oxide Fuel Cell with deposited Ce(Co,Cu)$O_{2-\delta}$ catalytic layer

Such prepared fuel cells were mounted in a measurement rig [18]. They were heated up to 800 °C with argon delivered to the anode side and then, in order to reduce nickel oxide, humidified hydrogen (3% H_2O) was supplied at 800°C for 30 min and further at 750°C for 20 h. After this time the hydrogen was replaced by wet synthetic biogas (3% H_2O) consisting of methane and carbon dioxide mixed at a volume ratio of 60/40. The total flow rate of the gas mixture was 30 cm^3 min^{-1}. Two types of electrical measurements were collected during fuel cell operation in biogas: a current density versus voltage and a current density versus time at 0.65 V for the time 120 h at 750 °C. A scheme presenting a general procedure of the experiment applied in this work is shown in Fig.2.

Simultaneously with electrical tests, an analysis of the composition of outlet gases from SOFC was performed using a Fourier Transformed Infrared Spectroscopy (Perkin Elmer Spectrum 100). Concentrations of methane, carbon dioxide and carbon monoxide were analyzed. Although H_2 gas is not visible in FTIR spectra, after a calibration process we were able to determine its concentration as a difference from 100% of summed CH_4, CO_2 and CO concentrations. Moreover, the conversion rates of CH_4 and CO_2 as well as the yields of H_2 and CO were calculated from the following expressions:

$$X_{CH_4} = \frac{n_{inCH_4} - n_{outCH_4}}{n_{inCH_4}} * 100\% \quad (12)$$

$$X_{CO_2} = \frac{n_{inCO_2} - n_{outCO_2}}{n_{inCO_2}} * 100\% \quad (13)$$

$$Y_{CO} = \frac{n_{outCO}}{n_{inCO_2} + n_{inCH_4}} * 100\% \quad (14)$$

$$Y_{H_2} = \frac{n_{outH_2}}{n_{inH_2O} + 2n_{inCH_4}} * 100\% \quad (15)$$

where n_{inCH4},n_{inCO2},n_{inH2O} and n_{outCO},n_{outH2} are the concentrations of respective inlet and outlet gases. *X* and *Y* are expressed in percentage. Conversion factor shows how much of studied gas was transformed during the catalytic processes, while yield informs us how much gas formed during catalytic reaction was found in the outlet stream with respect to the theoretical amount calculated from the chemical reactions [18].
A detailed description of the measuring system and analysis methods was reported elsewhere [19].

Fig.2: Procedure of the experiment.

3. Results and discussion

Properties of fabricated powders

The XRD patterns of all fabricated compounds are presented in Fig.3.

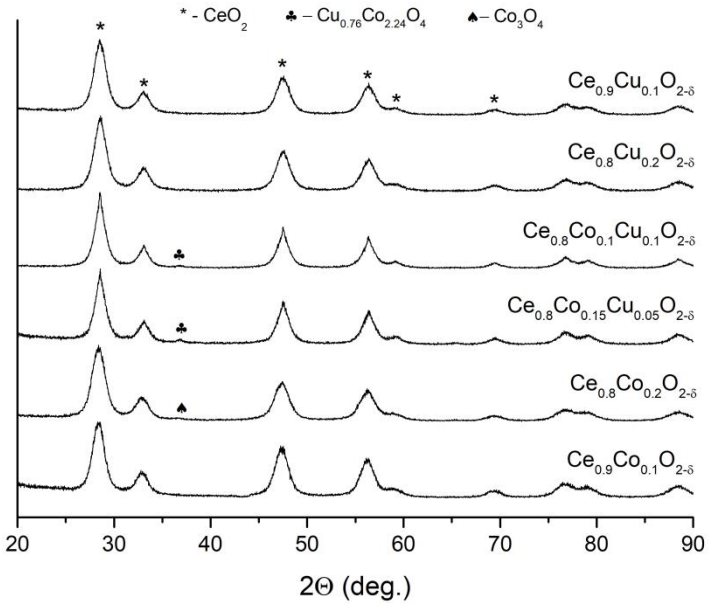

Fig.3: XRD patterns of fabricated Ce(Co,Cu)$O_{2-\delta}$ powders

They show that $CeO_{2-\delta}$ is a dominant phase, however in cobalt containing powders also some peaks which can be attributed to additional phases can be found. A small peak from Co_3O_4 is present in the XRD pattern of $Ce_{0.8}Co_{0.2}O_{2-\delta}$, whereas a trace of $Cu_{0.76}Co_{2.24}O_4$ presence is visible in XRD patterns of Co and Cu co-doped ceria compounds ($Ce_{0.8}Co_{0.1}Cu_{0.1}O_{2-\delta}$ and $Ce_{0.8}Co_{0.15}Cu_{0.05}O_{2-\delta}$). This indicates that in $Ce_{1-x}Cu_xO_{2-\delta}$ the solubility of Cu reaches 20 mol%, whereas in the case of co-doped with copper and cobalt ceria the total solubility of the dopants is lower than 20 mol%. In $Ce_{1-x}Co_xO_{2-\delta}$ the solubility limit is between 10 and 20 mol%. These values are much higher than the solubility limits of Cu and Co in ceria reported in the literature. For Co it is very low and equal to 3% [20] and for Cu it reaches 15% [21]. Interestingly, no traces of additional phases can be found in XRD pattern of $Ce_{0.8}Cu_{0.2}O_{2-\delta}$. It may result both from the resolution of the XRD measuring technique, segregation of nanocrystalline additional phases on the grain boundaries, as well from different synthesis method than that reported in the literature [4,5], what may change a solubility limit of particular elements in ceria. Moreover, according to the literature, the solid solubility limit can be enhanced by even few orders of magnitude, if the material is in the nanocrystalline state [22]. However, even if the solubility limit is exceeded and some additional phases are formed, or they segregate on the grain boundaries, they may not deteriorate the catalytic properties of fabricated materials. According to literature reports [23] the spinel Co_3O_4 has a high catalytic activity with respect to several complete oxidation reactions. It is due to the high mobility and the low binding energy of surface oxygen in this oxide. Similar behavior has been observed for binary cobaltites [23]. Some authors claim that these cobaltites may be more stable than the noble metals against catalytic poisons [23,24].

On the basis of XRD data also the size of crystallites was estimated using the Scherrer equation. The obtained results are presented in Table 2. They confirm that a reverse microemulsion synthesis method allowed to successfully fabricate nanocrystalline compounds. Among them, the biggest crystallites (ca. 7 nm) present both Cu and Co co-doped ceria compounds. The sizes of other compounds are comparable and close to 5 nm.

In Table 2 also an average size of grains taken from SEM analysis is presented for each compound. Sample SEM images of $Ce_{0.9}Co_{0.1}O_{2-\delta}$, $Ce_{0.9}Cu_{0.1}O_{2-\delta}$ and $Ce_{0.8}Co_{0.1}Cu_{0.1}O_{2-\delta}$ materials are presented in Fig.4. They indicate that all grains are uniform, round shaped and of nanometric size. However, in the $Ce_{0.8}Co_{0.1}Cu_{0.1}O_{2-\delta}$ powder some larger agglomerates of a size up to 0.7 μm can be found. These pictures are representative of all other fabricated compositions. An average size of grains is comparable and equal to 20 nm.

Table 2: Average size of crystallites (from XRD) and the average size of grains (from SEM) calculated for fabricated Ce(Co,Cu)$O_{2-\delta}$ powders

Compound	Size of crystallites (nm)	Size of grains (nm)
$Ce_{0.9}Cu_{0.1}O_{2-\delta}$	5.4±0.3	19±3
$Ce_{0.8}Cu_{0.2}O_{2-\delta}$	5.4±0.3	21±5
$Ce_{0.8}Co_{0.1}Cu_{0.1}O_{2-\delta}$	7.4±0.7	20±4

This work was presented during the 13th International Symposium on Systems with Fast Ionic Transport, Minsk, Belarus 03–07.07.2018

$Ce_{0.8}Co_{0.15}Cu_{0.05}O_{2-\delta}$	6.5±0.5	23±3
$Ce_{0.8}Co_{0.2}O_{2-\delta}$	4.7±0.4	25±4
$Ce_{0.9}Co_{0.1}O_{2-\delta}$	5.5±0.4	20±3

a) $Ce_{0.9}Co_{0.1}O_{2-\delta}$ b) $Ce_{0.9}Cu_{0.1}O_{2-\delta}$ c) $Ce_{0.8}Co_{0.1}Cu_{0.1}O_{2-\delta}$

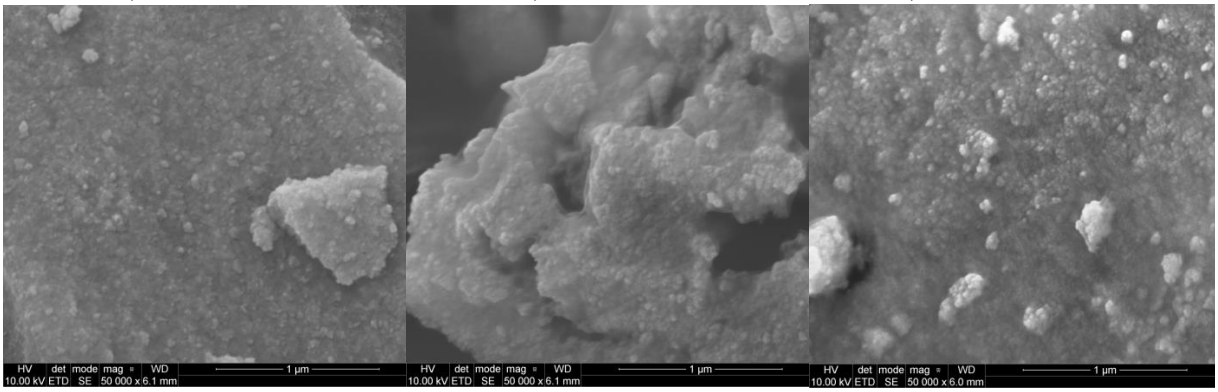

Fig.4: SEM images presenting nanosize powders of $Ce_{0.9}Co_{0.1}O_{2-\delta}$ (a), $Ce_{0.9}Cu_{0.1}O_{2-\delta}$ (b) and $Ce_{0.8}Co_{0.1}Cu_{0.1}O_{2-\delta}$ (c) compounds

Properties of fuel cells with additional catalytic layers

3.1. Electrical properties

The plots presenting power density values for fuel cells with different $Ce(Co,Cu)O_{2-\delta}$ anode layers measured at 0.65 V in various stages of the experiment are presented in Fig.5. Point "0" in the "time" axis depicts a moment in which a gas supplied to the anode side was switched from hydrogen to biogas. It can be seen that the power density in hydrogen (Fig.5) is quite unstable in time. This instability comes from some structural changes taking place on the anode side in the beginning of the exposure to high temperature in hydrogen. It agrees with literature reports [25]. During this time, opposite processes take place, e.g. ordering of metallic nickel in the structure of the anode, segregation of impurities, sintering of catalyst grains [25]. It is only after a few hours that we reach the equilibrium state of the system and more stable electrical parameters.

Another interesting observation is that the power densities of the fuel cells both in hydrogen and in biogas atmosphere differ from one another (Fig.5). In order to better understand the source of these differences also the I-V measurements were performed. The results for all investigated fuel cells at two stages of the experiment: in the beginning of operation in H_2 (Fig.6a) and after 90 hours of operation in biogas (Fig.6b) are presented. It is clear that except $Ce_{0.8}Co_{0.15}Cu_{0.05}O_{2-\delta}$ all compounds give comparable value of OCV in hydrogen (*c.a.* 1.03V) which is close to a theoretical value predicted by the Nernst equation. The slope of I-V curves for all compounds except $Ce_{0.8}Co_{0.15}Cu_{0.05}O_{2-\delta}$ in hydrogen is also comparable. We suppose that observed differences of the power densities in hydrogen may come not only from catalytic activity of a material but also from a microstructure of deposited layers. From Fig.6b one can see that after 90 hours of feeding with biogas the OCV for all fuel cells is lower than in hydrogen and equal to *c.a.* 0.97 V. This decrease is in agreement with both theoretical predictions and experimental results from other papers [26,27]. Since more than one electrochemical oxidation is possible in the system, the theoretical OCV in biogas is a combination of the different reactions taking place at the anode surface (equations 8-11) [27] and it should be lower than in pure hydrogen. The slope of I-V curves for all compounds in biogas is comparable.

Further analysis of Fig.5 indicates that for a particular amount of a single type of dopant (10 or 20 mol%) the power densities in hydrogen are comparable, but in general, a lower amount of dopant gives higher power density. Differences appear after switching to biogas. Layers of ceria doped with cobalt are more sensitive to biogas atmosphere and within the first 30 hours of operation in biogas show lower power density than fuel cells with Cu-doped ceria. In order to explain this phenomenon one can make a hypothesis that it may be caused by coking phenomenon which is more intensively catalyzed by cobalt than by copper [8]. This coking may lead to the deactivation of Ni catalyst and to the blocking of fuel diffusion to TPB. However, doping with cobalt stabilizes ceria in direct internal reforming conditions and thus a further deterioration of fuel cell with time (after 30 hours) is limited. A noticeable enhancement of electrical properties in DIR-SOFC conditions is observed

when Co and Cu co-doped ceria catalytic layers are applied. Both the fuel cells with the $Ce_{0.8}Co_{0.1}Cu_{0.1}O_{2-\delta}$ and $Ce_{0.8}Co_{0.15}Cu_{0.05}O_{2-\delta}$ layers show the highest power density and the best long-term stability in biogas atmosphere.

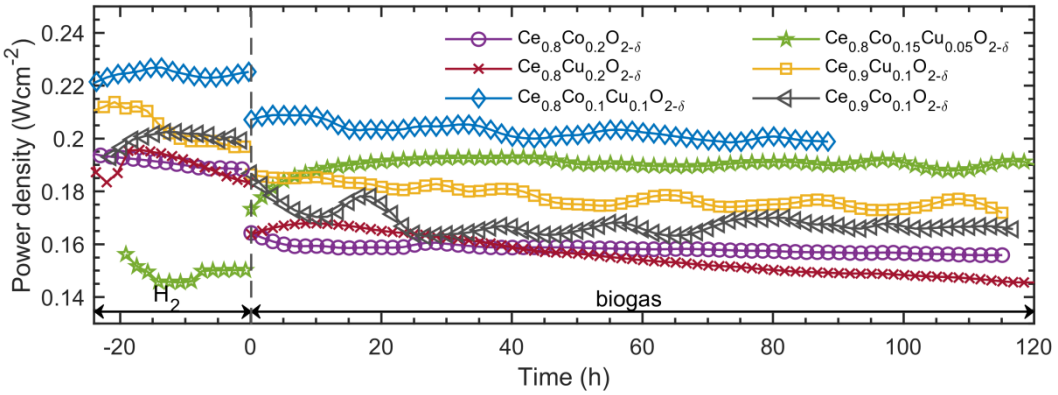

Fig.5: Power density as a function of time for fuel cells with the $Ce(Co,Cu)O_{2-\delta}$ anode catalytic layers.

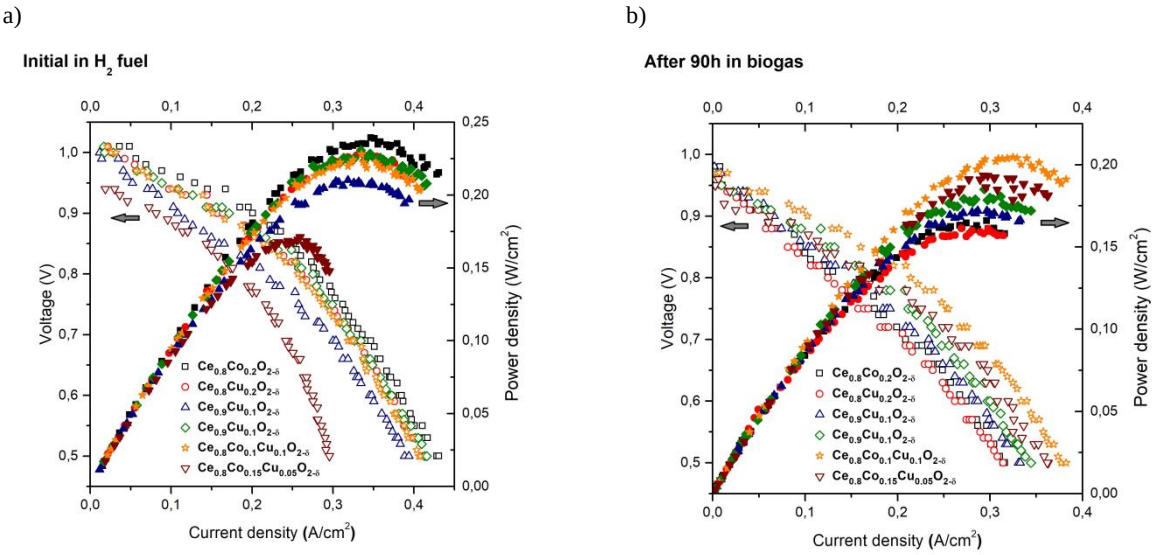

Fig.6: I-V curves for all investigated fuel cells at two stages of experiment: in the beginning of operation in H_2 (a) and after 90 hours feeding with biogas (b)

3.2. FTIR analysis of outlet gases

To better understand the influence of a particular catalytic layer on a direct internal reforming of biogas in investigated fuel cells an analysis of the composition of outlet gases was performed using the Fourier Transformed Infrared Spectroscopy. Plots of the conversion rate of methane and carbon dioxide versus time are presented in Fig.7. Plots showing a yield of carbon monoxide and hydrogen vs. time are shown in Fig.8. It can be found that Cu and Co co-doped ceria layers present the highest CH_4 conversion rate, simultaneously showing the lowest CO_2 conversion rate. In turn, layers with 20 mol% of a single type of dopant show the lowest CH_4 conversion rate and the highest conversion rate of CO_2. These observations correlate well with the analysis of CO yield. The highest CO yield occurs for Cu and Co co-doped ceria, and the lowest for layers with 20 mol% of a single type of dopant. For all investigated materials the H_2/CO yield ratio at a given stage of the experiment is always lower than 1 indicating that a reverse water-gas-shift reaction (reaction (2)) substantially proceeds.

The H_2 yield is the highest for $Ce_{0.8}Co_{0.2}O_{2-\delta}$, $Ce_{0.8}Cu_{0.2}O_{2-\delta}$ and $Ce_{0.8}Co_{0.15}Cu_{0.05}O_{2-\delta}$ layers. On the contrary to other catalytic parameters, it stabilizes after 30-40 hours of operation in biogas. In turn, a continuous decrease (lasting ca. 70 hours) of CH_4 and CO_2 conversion rates as well a decrease of CO yield indicate the

progressive catalyst deactivation process. After this time these parameters stabilize, and a state of electrochemical equilibrium is reached in the system. This indicates that coking phenomenon (mostly from reaction 5) leading to the deactivation of Ni catalyst and to the blocking of fuel diffusion to TPB is compensated by a removal of solid carbon. It takes place mostly via electrochemical oxidation of solid carbon (reaction 11). Remembering that biogas mixture supplied to an anode compartment is humidified (3% H_2O) and that additional amount of water is produced via methanation process (reaction 3) also a reverse of reaction (7) may occur enhancing a carbon removal. On the other hand, for high CO_2/CO ratio the equilibrium of reaction (6) is shifted to the direction of CO formation, suppressing carbon deposition through Boudouard reaction. All these phenomena reduce the carbon accumulation in the volume of Ni-YSZ anode [1].

Since both reforming products (H_2 and CO) can be electrochemically oxidized leading to the production of electricity (according to reactions 8 and 9), their formation within direct internal reforming of biogas is desired. Although H_2 oxidation is considerably faster than that of CO, it will have a key contribution to the electrical performance of a fuel cell. It should be remembered that the yield parameter expressed by reactions (14) and (15) provides information about amount of gas formed during catalytic reaction that was found in the outlet stream with respect to the theoretical amount calculated from the chemical reactions. If more hydrogen is utilized within an electrochemical oxidation according to the reaction (8), then less hydrogen will be found in the outlet stream and we will obtain lower H_2 yield. Therefore, one may suggest that lower H_2 yield may result from more intensive electrochemical reaction (8). As this reaction performs faster than (9), the CO yield may by higher (less CO is electrochemically oxidized). It agrees with power density measurements. The highest CO yield and much lower H_2 yield is obtained for both Cu and Co co-doped ceria layers and these materials present the highest power density and the best long-term stability.

a)

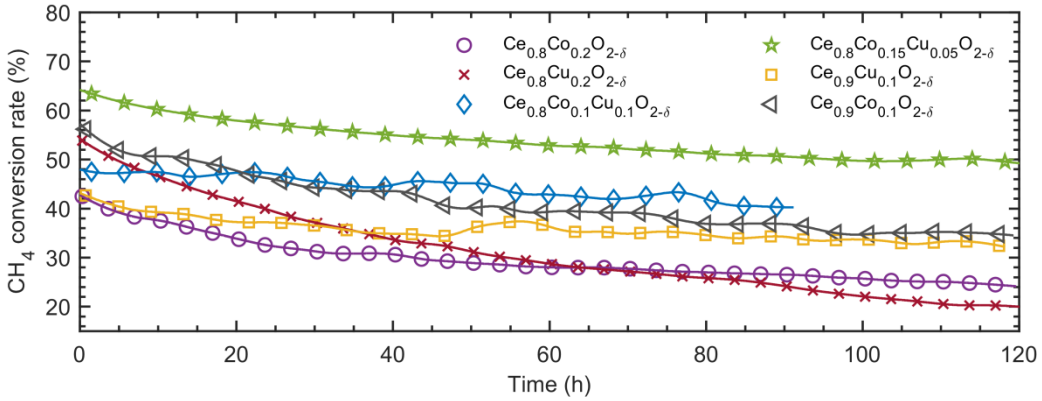

b)

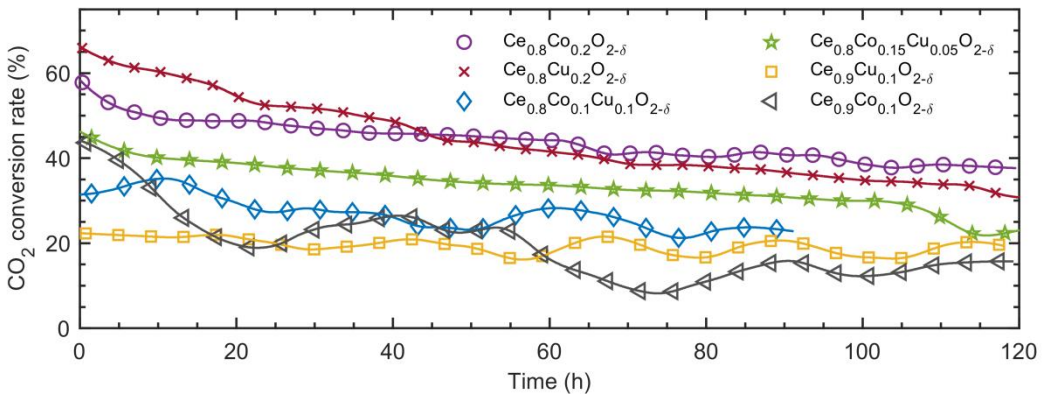

Fig. 7: Conversion rate of methane (a) and carbon dioxide (b) as a function of time.

a)

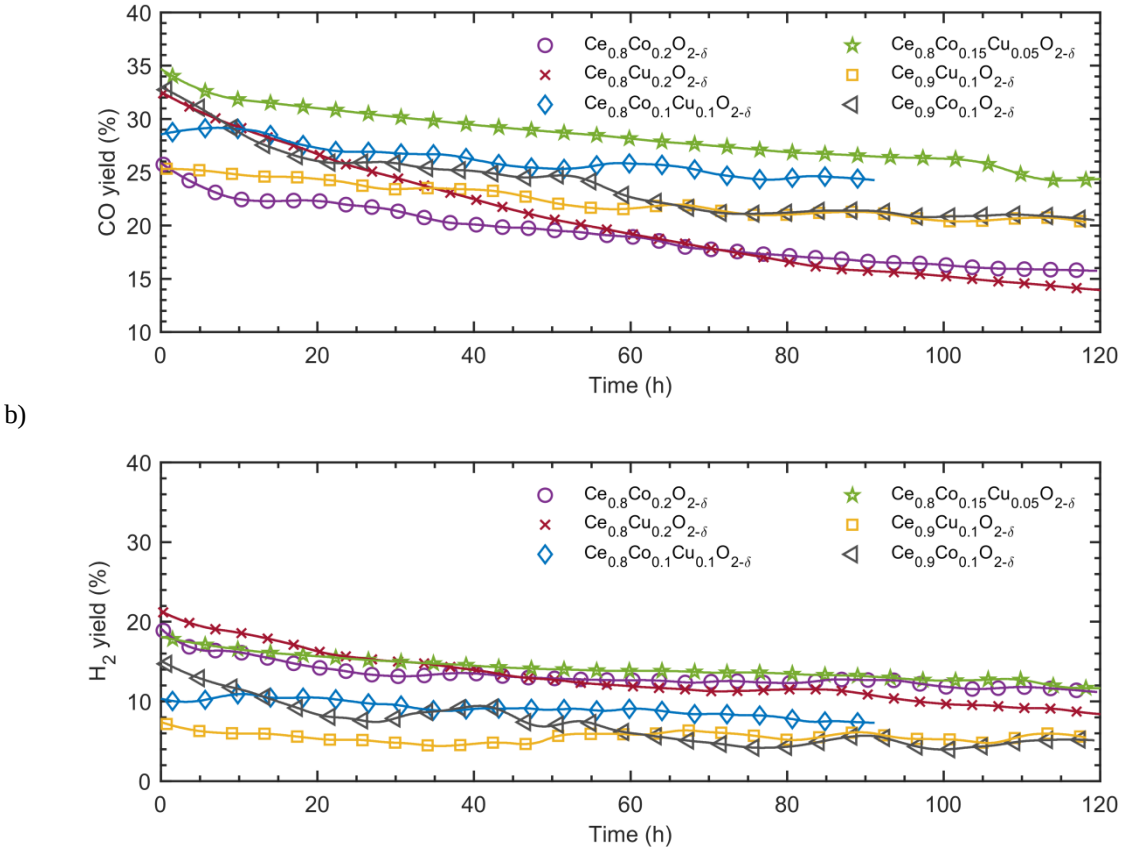

Fig.8: Yield of carbon monoxide (a) and hydrogen (b) as a function of time.

Properties of catalytic layers after operation in biogas

Finally, the analysis of the properties of deposited layers was performed after the operation in biogas atmosphere. The SEM images of layers of three representative compositions: $Ce_{0.9}Co_{0.1}O_{2-\delta}$, $Ce_{0.9}Cu_{0.1}O_{2-\delta}$ and $Ce_{0.9}Co_{0.1}Cu_{0.1}O_{2-\delta}$ are presented in Fig.9. They clearly indicate that although all these materials were nanocrystalline powders after a fabrication process (as shown in Fig.4), the grains grew to a different extent depending on a type o dopant. The smallest grains (ca. 100-200 nm) are visible in cobalt-doped ceria layer and the biggest (up to 2 μm) in Cu-doped ceria. When both Co and Cu dopants are added to ceria, then a grain growth is limited, and we obtain grains of intermediate size (ca. 200-400 nm) and a uniform, round shape. This is a desirable effect because smaller grains have a bigger catalytically active surface area for reforming reactions.

a) $Ce_{0.9}Co_{0.1}O_{2-\delta}$ b) $Ce_{0.9}Cu_{0.1}O_{2-\delta}$ c) $Ce_{0.8}Co_{0.1}Cu_{0.1}O_{2-\delta}$

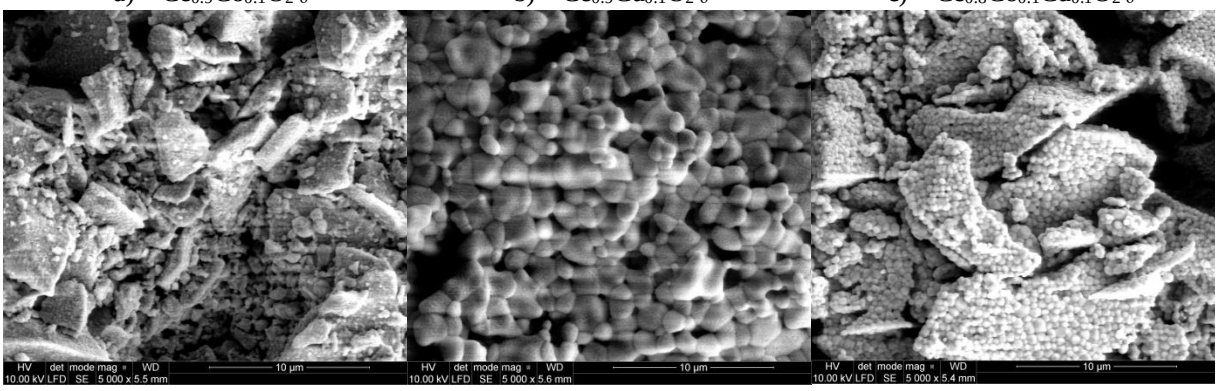

Fig.9: SEM images presenting structure of $Ce_{0.9}Co_{0.1}O_{2-\delta}$ (a), $Ce_{0.9}Cu_{0.1}O_{2-\delta}$ (b) and $Ce_{0.8}Co_{0.1}Cu_{0.1}O_{2-\delta}$ (c) catalytic layers after operation in biogas

To determine a phase composition of layers after the operation in biogas the XRD measurement was performed. The XRD pattern of $Ce_{0.8}Co_{0.1}Cu_{0.1}O_{2-\delta}$ is shown in Fig.10.

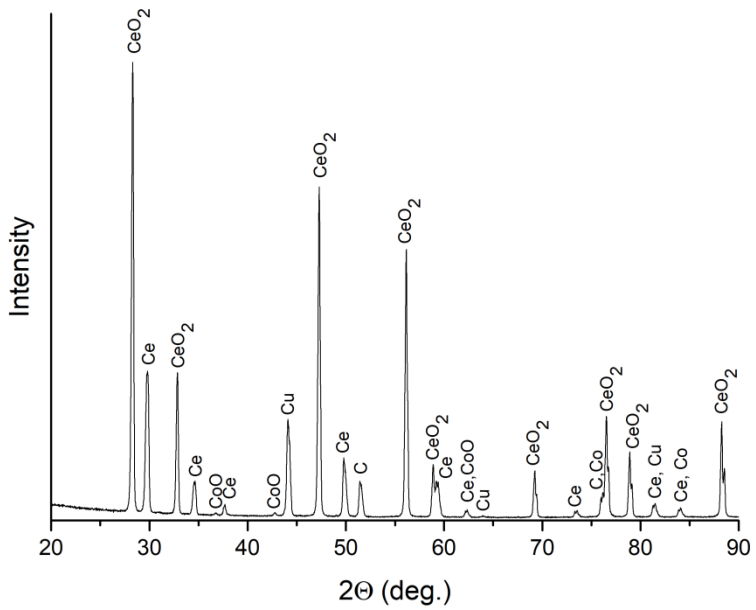

Fig10: XRD pattern of $Ce_{0.8}Co_{0.1}Cu_{0.1}O_{2-\delta}$ catalytic layer after operation in biogas

It should be noticed that apart from the peaks representing the CeO_2 phase also some peaks of Ce, Cu, Co and CoO can be found. This is a result of the reduction process taking place in fuel cell conditions (800 °C in H_2, 750 °C in biogas). Also, the $Cu_{0.76}Co_{2.24}O_4$ phase was decomposed and reduced, because no peaks which can be attributed to this phase can be found in the XRD pattern. According to H_2-TPR profiles presented in the literature [8] the presence of CuO favors the reduction of Co_3O_4 to CoO, enabling it to take place at low temperature (ca. 290 °C). It was ascribed as a strong synergetic effect of copper and cobalt when they were deposited by a co-impregnation method. We suppose that a similar synergetic effect may take place in our Co and Cu-doped ceria compound. The existence of Cu and Co in a metallic form is desirable, because in this form they present the highest catalytic activity for electrochemical oxidation of hydrogen that is produced within a biogas reforming. On the other hand, cobalt is an active component for C-C chain growth [8]. That is why also a peak from solid carbon (C) can be found in the XRD pattern. Deposition of carbon is an undesired phenomenon because it leads to the deactivation of Ni catalyst. However, it may not be a problem if the deposition of carbon occurs only in the catalytic layer, not in the Ni-YSZ anode, as was observed in our other paper [12]. This let us conclude that although a presence of cobalt in ceria is desired for biogas reforming, its content should not be too high to prevent a permanent damage of catalytic layer by carbon deposition.

4. Conclusions

Various nanocrystalline compounds of Co and Cu co-doped ceria (with up to 20 mol.% of dopants) were fabricated by the reverse microemulsion synthesis method. They were deposited in a form of layers on the surface of SOFC anode in aim to act as electrochemically active materials for biogas reforming process. It was found that among fabricated compounds both Cu and Co co-doped ceria layers give the best electrical parameters of a fuel cell and the best long-term stability. These materials give also the highest conversion rate of methane and the highest yield of carbon monoxide. Moreover, co-doping prevents an undesirable grain growth of catalytic material, allowing to obtain a high surface area for catalytic reactions.

Acknowledgments

Authors would like to thank Mr Pawel Szulczewski for his help in samples preparation. This work was supported by the National Science Center under the grant No. NCN 2017/26/D/ST8/00822 and by the Foundation for Polish Science (FNP) within the START scholarship.

References

[1] T. Dang-Long, T. Quang-Tuyen, Y. Shiratori, Catalytic and electrochemical behaviour of solid oxide fuel cell operated with simulated-biogas mixtures, AIP Conference Proceedings 1737, 060012 (2016)
[2] Y. Shiratori, T. Ijichi, T. Oshima, K. Sasaki, Int J. Hydrogen Energy, Vol. 35, 7905–7912 (2010).
[3] M.V. Iyer, L.P. Norcio, E.L. Kugler, D.B. Dadyburjor, Ind. Eng. Chem. Res., Vol. 42, 2712–2721 (2003)
[4] G.Ding, T.Gan, J.Yu, P.Li, X.Yao, N.Hou, L.Fan, Y.Zhao, Y.Li, Catalysis Today, 298 (2017) 250-257
[5] A.A.A. da Silva, N. Bion, F. Epron, S. Baraka, F.C. Fonseca, R.C. Rabelo-Neto, L.V. Mattose, F.B. Noronha, Applied Catalysis B: Environmental **206** (2017) 626–641
[6] H. He, J.M. Hill, Applied Catalysis A: General **317** (2007) 284–292.
[7] H.S. Bengaard, J.K. Norskov, J. Sehested, B.S. Clausen, L.P. Nielsen, A.M. Molenbroek, J.R. Rostrup-Nielsen, Journal of Catalysis **209** (2002) 365–384.
[8] S.Deng, W.Chu, H.Xu, L.Shi, L.Huang, Journal of Natural Gas Chemistry 17(2008)369–373
[9] P.Boldrin, E.Ruiz-Trejo, J.Mermelstein, J.M. Bermúdez Menéndez, T. Ramírez Reina, Nigel P. Brandon, Chem. Rev. 116, 22, 13633-13684
[10] McIntosh, S.; Vohs, J. M.; Gorte, R. J., Electrochim. Acta 2002, 47 (22−23), 3815−3821
[11] Kim, H.; Lu, C.; Worrell, W. L.; Vohs, J. M.; Gorte, R. J., J. Electrochem. Soc. 2002, 149 (3), A247−A250
[12] D. Szymczewska, J.Karczewski, B. Bochentyn, A.Chrzan, M.Gazda, P.Jasiński, Solid State Ionics 271 (2015) 109–115
[13] Grgicak, C. M.; Green, R. G.; Giorgi, J. B., J. Power Sources 2008, 179 (1), 317−328
[14] O'Brien, J. S.; Giorgi, J. B., J. Power Sources 2012, 200, 14−20.
[15] Orlyk, S. N.; Shashkova, T. K., Kinet. Catal. 2014, 55 (5), 599−610.
[16] Kaur, G.; Basu, S. Fuel Cells 2014, 14 (6), 1006−1013
[17] Tz. Kraia, S. Wachowski, E. Vøllestad, R. Strandbakke, M. Konsolakis, T. Norby, G.E. Marnellos, Solid State Ionics 306 (2017) 31-37
[18] Dunst K.M., Karczewski J., Miruszewski T., Kusz B., Gazda M., Molin S., Jasinski P., Solid State Ionics 251 (2013) 70–77
[19] Chlipała M., Białk O., Wang S.-W., Jasiński P., Bochentyn B.: In situ analysis of composition of exhaust gases from a Solid Oxide Fuel Cell fed by biogas using Fourier Transform Infrared Spectroscopy. Submitted to International Journal of Hydrogen Energy, in review.
[20] Jud E., Zhang Z., Sigle W., Gauckler L. J.: Microstructure of cobalt oxide doped sintered ceria solid solutions. J Electroceram 16, 2006, p.191-197.
[21] Zimmer P., Tschöpe A., Birringer R.: Temperature-Programmed Reaction Spectroscopy of Ceria- and Cu/Ceria-Supported Oxide Catalyst. Journal of Catalysis 205, 2002, p.339-345.
[22] J.C.M. Li, Microstructure and properties of materials, 1996, Science, https://doi.org/10.1142/2882
[23] D. Klissurski, E. Uzunova, Journal of Materials Science 29 (1994) 285-293
[24] A. Crucq and A. Frennet, "Studies in surface science and catalysis, Vol. 30, Catalysis and automotive pollution control" (Elsevier, Amsterdam, 1987)
[25] M.S.Khan, S.-B. Lee, R.-H. Song, J.-W. Lee, T.-H. Lim, S.-J. Park, Fundamental mechanisms involved in the degradation of nickel–yttria stabilized zirconia (Ni–YSZ) anode during solid oxide fuel cells operation: A review, Ceramics International 42 (2016) 35–48
[26] A. Fuerte, R.X. Valenzuela, M.J. Escudero, L. Daza, International Journal of Hydrogen Energy, 39 (2014) 4060-4066
[27] M. J. Escudero, A. Fuerte, Fuel Cells 16 (2016) 3, 340–348